Research in Astronomy and Astrophysics

Abundances of 23 field RR Lyrae stars

To cite this article: Liu Shu *et al* 2013 *Res. Astron. Astrophys.* **13** 1307

View the article online for updates and enhancements.

You may also like

- CONSTRAINTS ON THE FORMATION OF THE GALACTIC BULGE FROM Na, Al, AND HEAVY-ELEMENT ABUNDANCES IN PLAUT's FIELD
Christian I. Johnson, R. Michael Rich, Chiaki Kobayashi et al.
- THE CHEMICAL COMPOSITION OF RED GIANT STARS IN FOUR INTERMEDIATE-AGE CLUSTERS OF THE LARGE MAGELLANIC CLOUD
Alessio Mucciarelli, Eugenio Carretta, Livia Origlia et al.
- Chemical Tagging N-rich Field Stars with High-resolution Spectroscopy
Jincheng Yu, Baitian Tang, José G. Fernández-Trincado et al.

This content was downloaded from IP address 186.79.173.142 on 28/02/2025 at 06:43

Research in Astron. Astrophys. **2013** Vol. **13** No. **11**, 1307–1329
http://www.raa-journal.org *http://www.iop.org/journals/raa*

***R**esearch in*
***A**stronomy and*
***A**strophysics*

Abundances of 23 field RR Lyrae stars * †

Shu Liu[1,2], Gang Zhao[1], Yu-Qin Chen[1], Yoichi Takeda[3] and Satoshi Honda[4]

[1] Key Laboratory of Optical Astronomy, National Astronomical Observatories, Chinese Academy of Sciences, Beijing 100012, China; *gzhao@nao.cas.cn*
[2] Graduate University of Chinese Academy of Sciences, Beijing 100049, China
[3] National Astronomical Observatory of Japan 2-21-1 Osawa, Mitaka, Tokyo 181-8588, Japan
[4] Nishi-Harima Astronomical Observatory, Center for Astronomy, University of Hyogo, 407-2, Nishigaichi, Sayo-cho, Sayo, Hyogo 679-5313, Japan

Received 2013 March 20; accepted 2013 April 23

Abstract We present stellar parameters and abundances of 15 elements (Na, Mg, Al, Si, Ca, Sc, Ti, V, Cr, Mn, Fe, Ni, Cu, Y and Ba) for 23 field RR Lyrae variables based on high-resolution ($R \sim 60\,000$) and high signal-to-noise (S/N~ 200) spectra obtained using the High Dispersion Spectrograph on the Subaru Telescope. Six stars in the sample have more than one spectrum observed at different pulsation phases. The derived abundance ratios of [X/Fe] for 14 elements (except for Ba) do not vary during the pulsation cycle. An interesting curve of [Ba/Fe] versus phase is detected for the first time and it shows decreasing [Ba/Fe] with increasing temperature at a given metallicity. Combining with data in the literature, abundances of most RR Lyrae stars as a function of [Fe/H] follow the same trends as those of dwarf stars, but [Sc/Fe] and [Y/Fe] ratios of RR Lyrae stars at solar metallicity are lower than those of dwarf stars. The kinematics of RR Lyrae stars indicate that three comparatively metal-rich RR Lyrae stars might originate from the thick disk and they show higher [α/Fe] ratios than RR Lyrae stars with thin disk kinematics. Among 23 RR Lyrae stars, two special objects are found with abnormal abundances; TV Lib has high [α/Fe], [Sc/Fe], [Y/Fe] and [Ba/Fe] ratios while TW Her has solar [α/Fe] but significantly lower [Sc/Fe], [Y/Fe] and [Ba/Fe] ratios as compared with other RR Lyrae stars.

Key words: techniques: spectroscopic — stars: abundances — stars: variables: RR Lyrae

1 INTRODUCTION

RR Lyrae variables are old, low mass stars located in the instability strip of the horizontal branch. Their short-period variability and relatively high luminosity make them easily identifiable even at large distances. Due to their small dispersion in intrinsic mean luminosity, RR Lyrae variables are often used as standard candles to measure distance. In addition to the distance scale, RR Lyraes play an important role in probing Galactic structure and formation. They are generally used to trace the

∗ Supported by the National Natural Science Foundation of China.

† Based on data collected by the Subaru Telescope, which is operated by the National Astronomical Observatory of Japan.

spatial and kinematic distribution of old stellar populations in the Galactic disk and halo components (Layden 1994, 1995a,b; Layden et al. 1996).

For a long time, RR Lyraes have commonly been used to study the chemical evolution of the disk and halo of the Milky Way. Preston (1959) adopted a low-resolution spectroscopic index ΔS to describe the relation between hydrogen and calcium K-line absorptions strengths. The index ΔS varies during RR Lyrae pulsational cycles, and it is used to identify times of light minimum ($\phi \sim 0.8$). High resolution studies have generally concentrated on the limited phase near minimum light, because of the relatively slow variations in effective photometric temperature that occur during these pulsation phases. In particular, Clementini et al. (1995) performed an abundance analysis of many elements for 10 RR Lyrae stars, and found that eight of them have [Fe/H] < -1.2, indicating they belong to the metal poor halo population. Lambert et al. (1996) studied two elements (Fe and Ca) in a sample of 18 RR Lyrae stars, and among these seven stars had [Fe/H] > -1.0. There have been very few works concentrating on the various elements that compose metal rich populations of RR Lyrae stars, which are thought to dominate the halo population. In this work we focus on probing the origin of the relatively metal-rich RR Lyraes. We present basic information about observations of our targets and describe the observation and data reductions in Section 2. Atmospheric parameters and abundances are derived in Section 3. In Section 4, we present the results of abundance and kinematic classification of the stars being studied. Concluding remarks are given in Section 5.

2 OBSERVATIONS AND DATA REDUCTION

The stars were selected from the literature with the main focus on finding metal-rich RR Lyrae stars. The observations were carried out on the night of 2004 June 27 with the High Dispersion Spectrograph (Noguchi et al. 2002) attached to the 8.2-m Subaru Telescope. Two CCDs with 2k$\times$4k pixels were employed to record spectra with a wavelength coverage of $5100 - 6400$ Å (blue) and $6500-7800$ Å (red), respectively. With a 0.6″ (300 μm) wide slit, the resolving power of the obtained spectra was $R \sim 60\,000$. To avoid any significant blurring of the spectrum, the exposure times were chosen to be no longer than 600 s and resulted in a mean signal-to-noise ratio S/N of $150 - 300$ for most of our spectra.

Our observations were carried out arbitrarily without pre-selection of the pulsation phase. Hence, the observed spectra have various phases, from phases near or at minimum light to phases near or at maximum light. In total, 36 high-resolution spectra for 23 RR Lyrae stars were obtained for this study. The basic parameters of the stars in our study are presented in Table 1. Of the 23 RR Lyrae stars, six stars (AO Peg, DH Peg, DX Del, RR Lyr, V445 Oph and VY Ser) have observations spanning multiple phases ($\geqslant 2$), while the remaining 17 stars have observations covering a single phase. Among the 23 stars in our study, 22 are RRab type and only one, DH Peg, is RRc type. Finally, DM Cyg, KX Lyr, RR Lyr, RS Boo, SW And, VX Her and VY Ser are Blazhko stars which exhibit long-period modulation of their light-curve amplitude, based on the recently published comprehensive list of Galactic field Blazhko stars (Skarka 2013).

The reduction of the spectra was performed with standard IRAF routines for bias substraction, flat-fielding, scattered light substraction, spectral extraction, wavelength calibration and continuum normalization. The radial velocity was derived by cross-correlating an individual spectrum with the template as described in Takeda et al. (2006). A portion of the spectra of RR Lyr (at ϕ = 0.36) and RS Boo (at ϕ = 0.31) is shown in Figure 1. The equivalent widths (EWs) of the stars in our study are measured using two methods. Due to variations in pulsation, some of our spectra show asymmetric line profiles. Thus we applied direct integration across the absorption line profile to derive the EW values from those spectra. Gaussian fitting was adopted for the lines at the phases with symmetric absorption profiles. To avoid error caused by damping wings, most of the lines used in the abundance analysis are weak and moderately strong lines with 5 mÅ $<$ EW $<$ 150 mÅ. In particular, for iron, we limited lines with EW to be in the range $10 - 120$ mÅ.

Table 1 Basic Information on Observations for Stars in our Study

Star	Period (d)	HJD [a]	Phase[b] (ϕ)	$v^c_{\rm rad}$ (km s^{-1})	Exp. time (s)	S/N[d]
AA Aql	0.361787	2453184.955	0.61	− 15.9	600	100
AO Peg	0.547243	2453185.031	0.77	−250.5	600	70
		2453185.039	0.79	−250.3	600	70
BR Aqr	0.481879	2453185.011	0.33	24.4	600	110
CI And	0.484726	2453185.094	0.45	25.4	600	60
CN Lyr	0.411382	2453184.825	0.53	34.0	600	150
DH Peg	0.255510	2453184.962	0.08	− 83.7	600	250
		2453185.048	0.41	− 66.1	600	310
		2453185.121	0.70	− 61.1	600	220
DM Cyg	0.419860	2453184.988	0.56	− 9.4	600	130
DO Vir	0.532723	2453184.779	0.36	6.8	600	40
DX Del	0.472617	2453184.893	0.17	− 73.1	600	290
		2453184.980	0.35	− 57.0	600	290
		2453185.069	0.54	− 44.4	600	240
IO Lyr	0.577123	2453184.902	0.26	−192.8	600	130
KX Lyr	0.440904	2453184.910	0.45	− 26.7	600	170
RR Cet	0.553028	2453185.083	0.18	− 94.4	600	200
RR Lyr	0.566838	2453184.796	0.90	−105.0	180	390
		2453184.882	0.05	− 96.2	180	490
		2453184.885	0.06	− 95.6	120	380
		2453184.971	0.21	− 79.1	120	330
		2453185.056	0.36	− 63.9	120	350
RS Boo	0.377339	2453184.740	0.31	− 7.0	600	210
SW And	0.442279	2453185.018	0.35	− 36.1	600	300
TV Lib	0.269624	2453184.935	0.40	− 84.1	600	80
TW Her	0.399600	2453184.814	0.12	− 33.3	600	170
UU Cet	0.606081	2453185.077	0.74	− 93.4	600	70
V413 Oph	0.449006	2453184.864	0.80	13.8	600	130
V440 Sgr	0.477479	2453184.878	0.15	− 91.1	600	260
V445 Oph	0.397023	2453184.791	0.77	6.4	600	140
		2453184.928	0.12	− 42.1	600	210
VX Her	0.455373	2453184.805	0.69	−350.7	600	170
VY Ser	0.714094	2453184.761	0.36	−142.8	600	240
		2453184.845	0.47	−135.5	600	270
		2453184.943	0.61	−129.5	600	140
		2453185.002	0.70	−125.7	600	110

Notes: [a] Heliocentric Julian Date at mid-exposure. [b] Pulsation phase (0 denotes the maximum of V magnitude). [c] Heliocentric radial velocity. [d] Mean signal-to-noise ratio.

We did two comparisons to inspect the reliability of our EWs. Firstly, we compared our EWs with those presented by Clementini et al. (1995). Clementini et al. (1995) measured EWs from the average spectra (close to the minimum light) of ten RR Lyrae stars with a large wavelength coverage of $3400 - 9900$ Å, resolving power of 38 000 and S/N $\sim 160 - 460$. The comparison of our EWs (at ϕ = 0.36) with Clementini et al. (1995) (at ϕ = 0.70) for the prototype star RR Lyr is shown in the left panel of Figure 2. Despite the phase difference between the spectra, EW values are in reasonable agreement with an rms error of 6.73 mÅ for 37 lines that are in common: $\mathrm{EW_{Clem95}} = -1.58 + 1.04\times$ $\mathrm{EW_{ThisWork}}$ mÅ. Secondly, a better internal consistency is found by comparing the EWs measured for the same lines from our spectra of RR Lyr observed at two successive phases ($\phi = 0.05$ and $\phi = 0.06$) but with different exposure times. A correlation of $\mathrm{EW}_{\phi=0.06} = -0.17 + 1.02\times \mathrm{EW}_{\phi=0.05}$ mÅ with an rms error of 1.69 mÅ is presented as follows (the right panel of Fig. 2) for 120 lines.

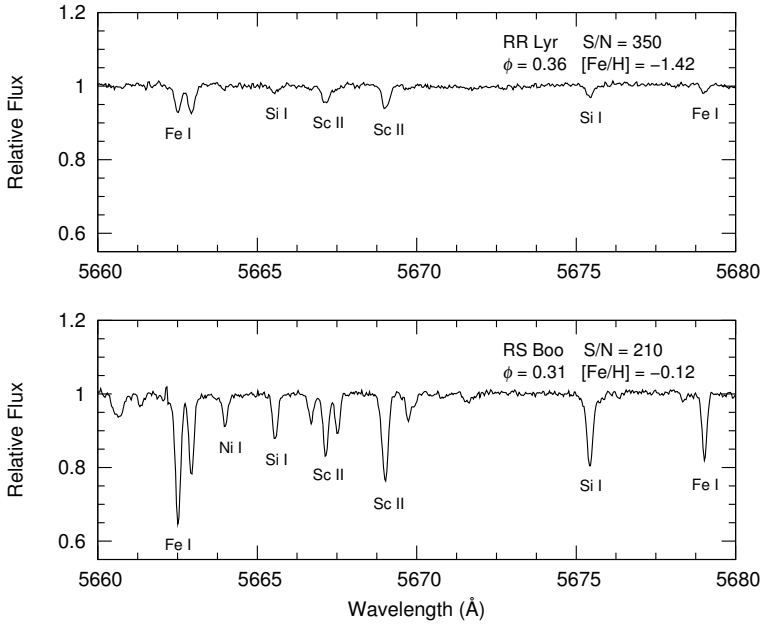

Fig. 1 A portion of sample spectra of RR Lyr and RS Boo.

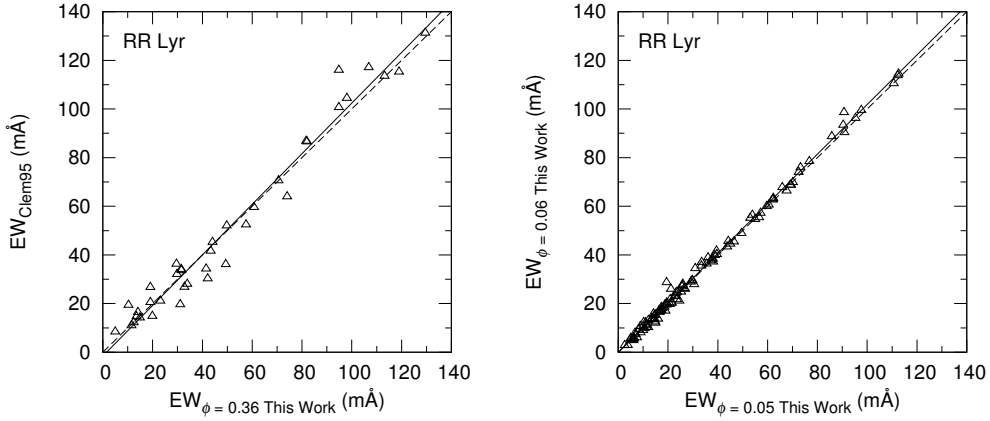

Fig. 2 Examining the consistency of equivalent width measurements, the dashed line represents a one-to-one relation while the thick line is the linear fit to the points. *Left panel*: Comparison of EWs in the present work with Clementini et al. (1995) for the common star RR Lyr. *Right panel*: Comparison for EW measurements of RR Lyr in two successive phases.

In this work, we estimated the specific pulsation phase of each spectrum by adopting the value of period and the time of light maximum (values which are nearest to our observation would be chosen among many observational maxima) from the GEOS RR Lyr Database[1] to obtain the pulsation ephemeris. The calculated phases for each of the 36 spectra are given in Table 1.

[1] *http://dbrr.ast.obs-mip.fr/*

3 MODEL ATMOSPHERIC PARAMETERS AND ABUNDANCE ANALYSIS

3.1 Atomic Data

The line list used for determination of stellar atmospheric parameters and abundance analysis is compiled from previous researches that focused on abundance analysis of RR Lyrae stars (Clementini et al. 1995; Lambert et al. 1996; Takeda et al. 2006). The $\log gf$ values are mainly adopted from high-precision laboratory measurements with several lines taken from Chen et al. (2000). The lines, $\log gf$ values and their references are listed in Table 2.

Table 2 Atomic Data and Measured Equivalent Widths for the First 10 Lines

Element	λ (Å)	EP (eV)	$\log gf$ (dex)	Ref.[a]	AA Aql ϕ=0.61	AO Peg ϕ=0.77	AO Peg ϕ=0.79	BR Aqr ϕ=0.33	.	.
Fe I	5083.339	0.960	−2.960	[1]	...	...	...	...	.	.
Fe I	5090.774	4.260	−0.440	[1]	58.1	18.7	26.5	46.3	.	.
Fe I	5096.998	4.280	−0.280	[3]	80.0	...	...	46.0	.	.
Fe I	5110.413	0.000	−3.760	[1]	104.1	63.5	66.0	74.5	.	.
Fe I	5121.639	4.280	−0.810	[1]	45.3	...	...	...	.	.
Fe I	5123.720	1.010	−3.070	[1]	79.1	27.1	38.6	49.5	.	.
Fe I	5125.117	4.220	−0.080	[3]	102.2	...	...	63.9	.	.
Fe I	5127.358	0.910	−3.310	[1]	65.8	...	22.7	39.5	.	.
Fe I	5131.470	2.220	−2.520	[1]	...	...	...	25.6	.	.
Fe I	5133.689	4.180	0.200	[3]	...	67.0	67.5	91.6	.	.
.	.	.	.	.	.	.	.	.	.	.
.	.	.	.	.	.	.	.	.	.	.
.	.	.	.	.	.	.	.	.	.	.

[a] References of adopted $\log gf$. A complete list of references is given in the online version of this table. Table 2 is available in its entirety in the online version (*http://159.226.170.66/liushu/rrlyr/rrl_ew_all.txt*).

3.2 Atmospheric Parameters

Being periodic variables, RR Lyrae stars have phase-dependent atmospheric parameters during their pulsation cycle. In most previous works, the observations were restricted to be at or near the minimum light when the atmosphere is known to be minimally affected by the pulsation. The execution of our observations is quite different. Without pre-phase-selection, spectra of stars in our study were arbitrarily observed at different phases. Thus, it is important to derive the atmospheric parameters of the star at the exact observation time. In this respect, Takeda et al. (2006) derived the atmospheric parameters ($T_{\rm eff}$, $\log g$, [Fe/H] and $v_{\rm t}$) with variations in the pulsation phases of four RR Lyrae stars (DH Peg, DX Del, RR Lyr, VY Ser) in our sample, by using the spectroscopic method with Kurucz (1993)'s ATLAS9 model grids, which could be a good touchstone for us to apply the same analysis in determination of atmospheric parameters of RR Lyrae stars at specific phases.

In the present work, model atmospheres are established by interpolating the ATLAS grids of Castelli & Kurucz (2003), which are based on assumptions of homogeneity, being plane-parallel and in local thermodynamic equilibrium (Castelli & Kurucz 2003). Effective temperature $T_{\rm eff}$ was estimated by requiring the Fe I abundances to be independent of the excitation potential (EP) of the lines used. To estimate the uncertainty of the adopted $T_{\rm eff}$, we increased the derived $T_{\rm eff}$ by a small amount until the $T_{\rm eff}$ being varied produced an obvious unacceptable trend in the derived mean Fe I abundances ($\Delta \log \epsilon$(Fe) exceeded a scatter of $\pm 1\sigma$) with EP. This method yielded an estimated average $T_{\rm eff}$ error of 100 K for stars in our study. The surface gravity $\log g$ was obtained

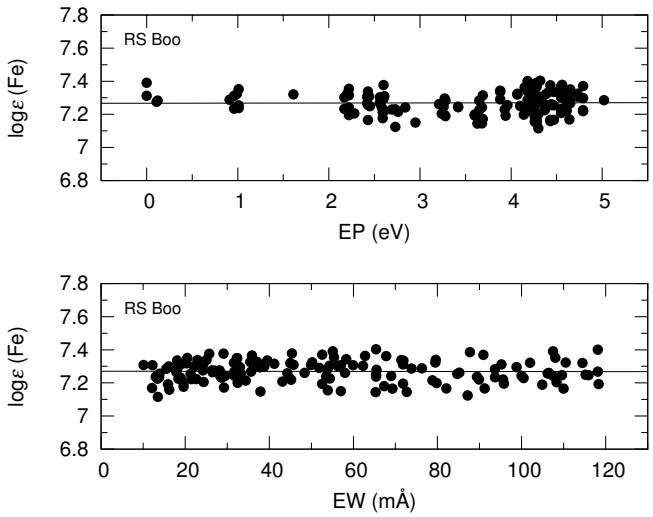

Fig. 3 Fe I abundances derived from individual Fe I lines for RS Boo as functions of excitation potential (EP, *upper*) and equivalent width (EW, *lower*). The regression lines represent the mean value of iron abundance. The determined parameters are $T_{\rm eff}$ = 6610 K, $\log g = 2.77$, [Fe/H] = -0.12 and $v_{\rm t}$ = 2.45 km s^{-1}.

by forcing the Fe I and Fe II to yield the same abundances (within uncertainties of 1σ internal scatter for both species). The uncertainty of $\log g$ was estimated by varying the $\log g$ value until the mean differences in abundance between Fe I and Fe II lines exceeded their uncertainty of $\sim$ 0.1 dex. The typical error in $\log g$ by this spectroscopic method is about 0.3 dex. Microturbulent velocity $v_{\rm t}$ was estimated in order to minimize the trend of Fe abundances from the Fe I lines with EWs. We inspect the uncertainty of $v_{\rm t}$ in the same manner as that applied on $T_{\rm eff}$ by assessing the trend of mean Fe I abundances with EWs. The errors of $v_{\rm t}$ are typically 0.3 km s^{-1}. The procedures are iterated until full consistency is reached when new a metallicity from spectroscopic analysis is obtained.

The upper and lower panels in Figure 3 show Fe I abundances of RS Boo as functions of excitation potential and equivalent width respectively. As can be seen, there is no trend in Fe I abundances either with the EP or with the EW in terms of lines. The derived atmospheric parameters for the 36 observed spectra are listed in Table 3.

3.3 Abundance Calculation and Uncertainties

Based on the established model atmospheres, the elemental abundances are calculated with the program ABONTEST8 by requiring the calculated EWs from the model to match the observed values. The solar abundances are derived with the same procedures as applied to our sample stars based on the Kurucz et al. (1984) Solar Flux Atlas. The chemical abundances of RR Lyrae stars are calculated with respect to the Sun in the differential analysis.

The uncertainties in abundance are estimated from two sources. One significant source of error is the random error of EWs, i.e. $\sigma_{\rm EW}$. This error can be estimated from the scatter in the elemental abundances from individual lines. The random error in the mean abundance is thus calculated as $\sigma_{\rm EW}/\sqrt{N}$, where N is the number of lines studied. For the elements that only have one line, we adopted the standard deviation $\sigma_{\rm EW}$ of Fe I (typically 0.07 dex) to represent the random error of those species. Another major source of error is the uncertainty in the stellar atmospheric parameters. In this work, we adopt the typical errors of model atmospheres with $\Delta T_{\rm eff}$ = 100 K, $\Delta \log g$ = 0.3 dex,

Table 3 Stellar Atmospheric Parameters

Star	Phase ϕ	$T_{\rm eff}$ (K)	$\log g$ (dex)	[Fe/H] (dex)	$v_{\rm t}$ (km s^{-1})
AA Aql	0.61	6550	2.70	−0.32	2.51
AO Peg	0.77	6323	2.50	−1.29	3.56
	0.79	6360	2.60	−1.22	2.86
BR Aqr	0.33	6515	2.52	−0.69	2.50
CI And	0.45	6373	2.50	−0.43	2.50
CN Lyr	0.53	6355	2.83	−0.04	3.05
DH Peg	0.08	7768	2.70	−1.02	1.95
	0.41	6950	2.58	−1.13	1.80
	0.70	7117	2.65	−1.14	1.66
DM Cyg	0.56	6415	2.85	0.03	3.15
DO Vir	0.36	6115	1.50	−1.57	2.49
DX Del	0.17	6673	2.67	−0.13	2.87
	0.35	6380	2.70	−0.13	2.74
	0.54	6310	2.83	−0.15	3.22
IO Lyr	0.26	6420	2.03	−1.35	2.80
KX Lyr	0.45	6495	2.75	−0.27	2.36
RR Cet	0.18	6650	2.20	−1.35	2.68
RR Lyr	0.90	7475	2.63	−1.31	2.47
	0.05	6620	2.05	−1.41	2.78
	0.06	6640	2.05	−1.39	2.87
	0.21	6250	1.98	−1.40	2.59
	0.36	6070	1.96	−1.42	2.57
RS Boo	0.31	6610	2.77	−0.12	2.45
SW And	0.35	6735	2.68	−0.07	2.83
TV Lib	0.40	6620	2.78	−0.43	2.02
TW Her	0.12	7465	2.38	−0.35	2.93
UU Cet	0.74	6250	2.38	−1.36	3.52
V413 Oph	0.80	7120	2.37	−0.75	2.83
V440 Sgr	0.15	7400	2.15	−1.18	2.84
V445 Oph	0.77	6495	2.95	0.14	3.65
	0.12	7140	2.92	0.13	2.97
VX Her	0.69	6300	2.25	−1.33	2.50
VY Ser	0.36	5998	1.83	−1.85	2.41
	0.47	5983	1.90	−1.83	2.48
	0.61	6113	1.93	−1.82	2.68
	0.70	6127	1.80	−1.80	3.00

Δ[Fe/H] = 0.1 dex and $\Delta v_{\rm t}$ = 0.3 km s^{-1} for all the stars in our study and estimated the uncertainty of abundance by varying the derived parameters plus/minus errors. We quote the total uncertainty for each element as the quadratic sum of the errors in abundance from atmospheric parameters and EWs. The corresponding uncertainties in abundance of RR Lyr ($\phi = 0.36$) and RS Boo ($\phi = 0.31$) are listed in Tables 4 and 5 as two typical cases, respectively.

In principle, Sc, V and Mn lines are affected by hyperfine splitting (HFS) and abundances for these elements could be improved by taking into account the effect of HFS. However, we noticed a recent study in which the variations of equivalent width of Mn I λ6013.5 and λ6021.8 induced by HFS were less than 1% for giants in ω Cen as shown in Cunha et al. (2010) by adopting the data on HFS from Prochaska et al. (2000). In our spectra, since most of the lines for Sc and Mn adopted are weak with EW values less than 50 mÅ, the HFS effect on these lines could be small. In addition, V lines of stars in our study are very weak (5.0 mÅ $\leqslant$ EW $\leqslant$ 14.0 mÅ) and thus the effect of HFS can be quite small. Considering the fact that the line-to-line scatter of individual elements is small for all stars, we can expect the effect of HFS to be insignificant in our results for the three species.

Table 4 Uncertainties in Abundance for Various Elements in RR Lyr ($\phi = 0.36$)

Elem.	ΔT +100 K	$\Delta \log g$ +0.30	Δ[Fe/H] +0.10	$\Delta v_{\rm t}$ +0.30	$\frac{\sigma_{\rm EW}}{\sqrt{N}}$	$\sigma_{\rm tot}$
Fe I	0.07	0.00	0.01	−0.02	0.01	0.07
Fe II	0.01	0.10	0.00	−0.03	0.03	0.11
Na I	0.04	−0.01	0.01	−0.01	0.06	0.07
Mg I	0.05	0.00	0.00	−0.03	0.13	0.14
Si I	0.04	0.00	0.00	0.00	0.03	0.05
Ca I	0.05	−0.01	0.00	−0.03	0.03	0.07
Sc II	0.04	0.10	0.00	−0.01	0.02	0.11
Ti I	0.08	−0.03	0.00	−0.01	0.04	0.09
Ti II	0.03	0.10	0.00	−0.02	0.04	0.11
Cr I	0.08	0.00	0.00	−0.03	0.04	0.09
Cr II	0.00	0.10	0.00	−0.01	0.04	0.11
Mn I	0.06	0.00	0.00	0.00	0.05	0.08
Ni I	0.06	0.00	0.00	0.00	0.02	0.06
Y II	0.05	0.10	0.01	0.00	0.01	0.11
Ba II	0.06	0.11	0.00	−0.07	0.14	0.20

Table 5 Uncertainties in Abundance for Various Elements in RS Boo ($\phi = 0.31$)

Elem.	ΔT +100 K	$\Delta \log g$ +0.30	Δ[Fe/H] +0.10	$\Delta v_{\rm t}$ +0.30	$\frac{\sigma_{\rm EW}}{\sqrt{N}}$	$\sigma_{\rm tot}$
Fe I	0.06	−0.01	0.01	−0.04	0.01	0.07
Fe II	0.01	0.10	0.00	−0.04	0.02	0.11
Na I	0.04	−0.01	0.00	−0.02	0.07	0.08
Mg I	0.04	−0.01	0.00	−0.05	0.07	0.10
Al I	0.04	−0.01	0.00	−0.01	0.06	0.07
Si I	0.04	−0.01	0.00	−0.02	0.01	0.05
Ca I	0.05	−0.01	0.00	−0.07	0.04	0.10
Sc II	0.04	0.10	0.01	−0.01	0.04	0.12
Ti I	0.08	0.00	0.01	0.00	0.03	0.09
Ti II	0.03	0.11	0.01	−0.03	0.04	0.12
V I	0.10	0.00	0.03	0.00	0.03	0.11
Cr I	0.07	0.00	0.00	−0.08	0.06	0.12
Cr II	0.01	0.11	0.01	−0.03	0.02	0.12
Mn I	0.06	−0.01	0.00	−0.02	0.04	0.08
Ni I	0.06	−0.01	0.00	−0.02	0.01	0.06
Y II	0.04	0.10	0.00	−0.02	0.05	0.12
Ba II	0.05	0.10	0.00	−0.12	0.12	0.20
Cu I	0.08	−0.01	0.00	−0.02	0.06	0.10

To inspect the variation in abundance caused by HFS of Sc, V and Mn for our stars, we selected five representative stars and calculated abundances by adopting data on HFS from the Kurucz webpage[2] and obtained the typical corrections for the effect of HFS of -0.01 for Sc, 0.00 for V and -0.03 for Mn. By using the same lines, the effects of HFS in the three species were also inspected in solar spectra and the corrections for Sc and V were both -0.02, which were similar to those of our stars and could be neglected. For Mn, the correction for HFS was -0.23 for the Sun, larger than that of our stars. Note that the ratios of [Mn/Fe] for stars in our study were 0.15 lower than the solar value (as can be seen in Fig. 7). By adopting differential corrections for HFS in Mn with respect to the Sun, we could adjust the zero point of [Mn/Fe] ratios for our stars by adding 0.19 to the solar metallicity

[2] *http://kurucz.harvard.edu/LINELISTS/GFHYPERALL/*

and thus our Mn abundance is more consistent with that of dwarf stars. Therefore, we concluded that the effect of HFS in Sc, V and Mn lines for our stars was insignificant.

3.4 Comparison With Previous Investigations

Based on the same set of data, Takeda et al. (2006) derived stellar parameters and [O/Fe] ratios for four RR Lyare stars that had multiple observations at different phases. We found consistent stellar parameters between the two works with deviations in $T_{\rm eff}$ of 100 K, in $\log g$ of 0.2 dex and in [Fe/H] of 0.05 dex. Note that we have carried out an independent abundance analysis and made some improvements to the analysis procedure by including more lines for Fe I and Fe II species and adopting new models by Castelli & Kurucz (2003). In particular, we compiled the line list from three sources (Clementini et al. 1995; Lambert et al. 1996; Takeda et al. 2006) and weak lines with EWs of $10-15$ mÅ were adopted, which were not included in Takeda et al. (2006), since our method of data reduction (spectral continuum normalization and EW measurement) can provide reliable EWs below 5 mÅ . These improvements provided more reliable stellar parameters and abundances in our work. For example, the inclusion of weak lines with EWs of $10-15$ mÅ improved the determination of microturbulence since they are least affected by varying microturbulence and would improve the temperature determination somewhat in the sense that some of them have low excitation potentials, which are few and important in the determination of temperature.

The comparison of our stellar parameters with other works in the literature is rather difficult since they (temperature, gravity and probably microturbulence) vary during the pulsation cycle and the spectra in different works were observed at different phases. There is a detailed discussion on stellar parameters from different works for the prototype RR Lyr by Kolenberg et al. (2010), and our result is consistent with their values as well as values published by Takeda et al. (2006). Alternatively, it will be more reasonable in the comparison of the derived abundance in different works in the sense that most elemental abundances of RR Lyrae stars will not change at different phases. There are four common stars in both the present work and in Fernley & Barnes (1996), and the deviation is ~ -0.15 for [Fe/H] and ~ 0.10 for [Ca/Fe]. The deviations between this work and Lambert et al. (1996) are about -0.30 in [Fe/H] and -0.06 in [Ca/Fe]. There are eight common stars with Clementini et al. (1995) and we found a deviation of -0.02 in [Fe/H] and even smaller for other elements. The deviations of our values from those of Fernley & Barnes (1996) and Lambert et al. (1996) come from the different methods adopted to determine temperatures in the abundance analysis. For RR Lyrae, there are spectra observed at a similar phase (ϕ = 0.35 in Lambert et al. versus ϕ = 0.36 in our work) and we found a $T_{\rm eff}$ that is higher by 130 K and $\log g$ that is higher by 0.33 dex in Lambert et al. (1996), which explains the significant deviation of 0.3 in [Fe/H] between the two works. We noticed that For et al. (2011) investigated the physical properties of RR Lyrae stars by comparing them with those presented in Lambert et al. (1996) and Clementini et al. (1995) in the $T_{\rm eff}-\log g$ plane, and they showed a large star-to-star scatter in the Lambert et al. (1996) samples. Our values are very consistent with those in Clementini et al. (1995), as well as those in For et al. (2011) in the comparison of temperature between the photometric and spectroscopic methods. We assumed that the spectroscopic method is favorable because it is based on high quality data and large numbers of iron lines. Although For et al. (2011) recently reported the effect of the parameters on the initial guess of temperatures, we have checked that all of our stars have convergent parameters starting from different initial parameters.

The derived relative abundances of 15 elements (Na, Mg, Al, Si, Ca, Sc, Ti, V, Cr, Mn, Fe, Ni, Cu, Y and Ba) are presented in Table 6 for six stars which have multiple observations, AO Peg, DH Peg, DX Del, RR Lyr, V445 Oph and VY Ser. Elemental abundances as a function of pulsation phase and metallicity for the six stars in our study (indicated by different symbols) are shown in Figures 4 and 5 respectively.

Table 6 Derived Abundances for Six Stars at Different Phases

Star	ϕ	[Fe/H]	[Na/Fe]	[Mg/Fe]	[Al/Fe]	[Si/Fe]	[Ca/Fe]	[Sc/Fe]	[Ti/Fe]	[V/Fe]	[Cr/Fe]	[Mn/Fe]	[Ni/Fe]	[Cu/Fe]	[Y/Fe]	[Ba/Fe]
AO Peg	0.77	−1.29	...	0.51	...	0.42	0.35	−0.01	0.27	...	−0.01	...	0.08	...	...	0.07
	0.79	−1.21	...	0.43	...	0.48	0.39	0.01	0.25	...	−0.02	...	0.06	...	...	0.22
DH Peg	0.08	−1.02	0.23	0.50	...	0.38	0.33	−0.03	0.26	...	−0.02	−0.40	0.02	...	−0.05	...
	0.41	−1.13	0.22	0.50	...	0.41	0.39	−0.01	0.31	...	−0.04	−0.37	−0.02	...	0.04	−0.25
	0.70	−1.14	0.29	0.51	...	0.41	0.41	0.02	0.33	...	0.03	...	0.02	...	0.00	−0.29
DX Del	0.17	−0.13	0.12	0.10	−0.26	0.08	0.11	−0.28	−0.10	−0.02	−0.08	−0.16	−0.04	−0.12	−0.39	−0.21
	0.35	−0.13	0.06	0.07	−0.21	0.06	0.04	−0.28	−0.06	−0.02	−0.04	−0.18	−0.02	−0.08	−0.36	−0.02
	0.54	−0.15	0.15	0.07	−0.10	0.10	0.02	−0.28	−0.06	−0.10	−0.07	−0.20	−0.01	−0.03	−0.35	0.01
RR Lyr	0.90	−1.31	...	0.26	...	0.19	0.31	−0.14	0.17	...	−0.12	...	...	...	...	−0.49
	0.05	−1.41	0.02	0.42	...	0.27	0.35	−0.07	0.23	...	−0.06	−0.47	−0.03	...	−0.13	−0.25
	0.06	−1.39	0.05	0.40	...	0.27	0.35	−0.09	0.25	...	−0.09	−0.47	−0.08	...	−0.12	−0.29
	0.21	−1.40	−0.05	0.41	...	0.32	0.38	−0.06	0.25	...	−0.09	−0.45	−0.07	...	−0.11	−0.05
	0.36	−1.42	−0.10	0.41	...	0.30	0.41	−0.03	0.22	...	−0.09	−0.45	−0.05	...	−0.14	0.08
V445 Oph	0.77	0.14	0.20	0.06	−0.13	0.02	0.20	−0.35	−0.26	...	−0.02	−0.10	−0.07	−0.02	−0.37	−0.13
	0.12	0.13	0.20	0.02	−0.26	0.06	0.18	−0.24	−0.23	...	−0.02	−0.09	−0.02	−0.14	−0.46	−0.40
VY Ser	0.36	−1.85	−0.02	0.44	...	0.38	0.47	−0.01	0.34	...	−0.08	−0.42	−0.09	...	−0.06	0.16
	0.47	−1.83	−0.10	0.49	...	0.22	0.50	−0.04	0.30	...	−0.03	...	−0.07	...	−0.07	0.18
	0.61	−1.82	−0.11	0.53	...	...	0.54	−0.03	0.36	...	0.02	...	−0.12	...	...	0.16
	0.70	−1.80	...	0.48	...	...	0.53	−0.03	0.26	...	0.06	...	0.01	...	...	0.14

4 RESULTS AND DISCUSSIONS

4.1 Abundances at Different Phases

One purpose of this work is to check the dependency of elemental abundance on phases for RR Lyrae stars. In Figures 4 and 5, we see that there is good consistency in the elemental abundances investigated in the present work at different phases of RR Lyrae stars. One exception is that [Ba/Fe] in RR Lyr stars shows large scatter at different phases, and the [Ba/Fe] ratio at ϕ = 0.90 is -0.45, 0.24 lower than the mean [Ba/Fe] = -0.21 in four of the phases. The trend of [Ba/Fe] versus phase is discussed in Section 4.2. Furthermore, the only RRc type star DH Peg, and two Blazhko stars, RR Lyr and VY Ser, follow the same trends as normal RR Lyrae stars with RRab type. This result was also recently reported by For et al. (2011), in that the abundance ratios, [X/Fe], of the α-elements, light odd-Z elements, and iron-peak elements show consistency throughout the pulsational cycles for both stars with and without the Blazhko effect. Their sample of RR Lyrae stars is within a narrow range of $-2.0 <$ [Fe/H] < -1.5 but the present work extends the validity of this result to a metal rich edge until the metallicity of [Fe/H] > 0.0. Also, For et al. (2011) indicate [Si I/Fe] declines and [Si II/Fe] increases with increasing $T_{\rm eff}$ between phase $0.8 - 1.0$, and they attributed this result to the neutral lines that are induced by a shock wave which partially disappears during these phases that are near their maximum. In the present work, the spectrum of RR Lyr at ϕ = 0.90 is the only spectrum observed at the post-maximum phase among our 36 spectra, and no obvious trend in [Si/Fe] versus phases has been found in Figure 4.

In summary, abundances of most elements in RR Lyrae stars observed at different phases can be used to trace the Galactic evolution like those in other stellar tracers. However, Si abundances should be used with caution if stars are observed at the phases of $0.8 - 1.0$ and Ba abundances should be avoided for the entire pulsation phase until its trends have been well explained.

4.2 The Dependance of Ba Abundance on $T_{\rm eff}$

As described above, [Ba/Fe] shows a large scatter at a given metallicity. We extend the analysis of [Ba/Fe] versus phase to all stars in our study. In the upper panel of Figure 6, Ba abundances of RR Lyr exhibit a trend that appears as a curve as a function of phase — a slightly rising trend during the phase section of $0.0 - 0.2$, reaching the peak at the phase of 0.4 and then a possible declining trend in the phase section of $0.8 - 1.0$. Moreover, [Ba/Fe] ratios show a large star-to-star scatter at a given metallicity, and we thus investigated their dependence on stellar parameters. We have found a decreasing trend of [Ba/Fe] with increasing temperatures as shown in the lower panel of Figure 6 for five different metallicity ranges. In particular, the prototype RR Lyr itself covers a large range in phase from 0.0 to 0.9, and it shows a very clear trend of decreasing [Ba/Fe] with increasing temperature while the metallicities at different phases are the same. The opposite behavior of AO Peg could be explained by the uncertainty in abundance. In addition, TW Her, which has a pronounced low [Ba/Fe] = -0.81 at the phase ϕ = 0.12, clearly follows the decreasing trend with increasing $T_{\rm eff}$.

The explanation for the dependence of [Ba/Fe] on $T_{\rm eff}$ is unknown and needs further investigation. One may wonder if the effect of non-local thermodynamic equilibrium (NLTE) on Ba abundances is the reason. Unfortunately, no such study for RR Lyrae stars can be found in the literature. For dwarf stars, Mashonkina et al. (1999) calculated the NLTE correction to be ~ -0.03 of Ba lines λ5853 for cool stars with [Fe/H] < -1.0. Andrievsky et al. (2009) investigated the NLTE effect of Ba lines for λ5853 for metal-poor stars with [Fe/H] < -2.0 and the NLTE correction as a function of temperature is 0.011 per 100 K. The NLTE result for the other Ba line λ6141 which is adopted in our work is not available in both of the two studies. For more metal-rich ranges, Mishenina et al. (2009) found the NLTE correction of Ba abundances for giants in M10 ([Fe/H] $= -1.5$) and M71 ([Fe/H] $= -0.8$) was within 0.1. If these results could be applied to RR Lyrae stars, we can expect a variation of Ba abundances with temperature from 6000 K to 7400 K, as shown in Figure 6, which

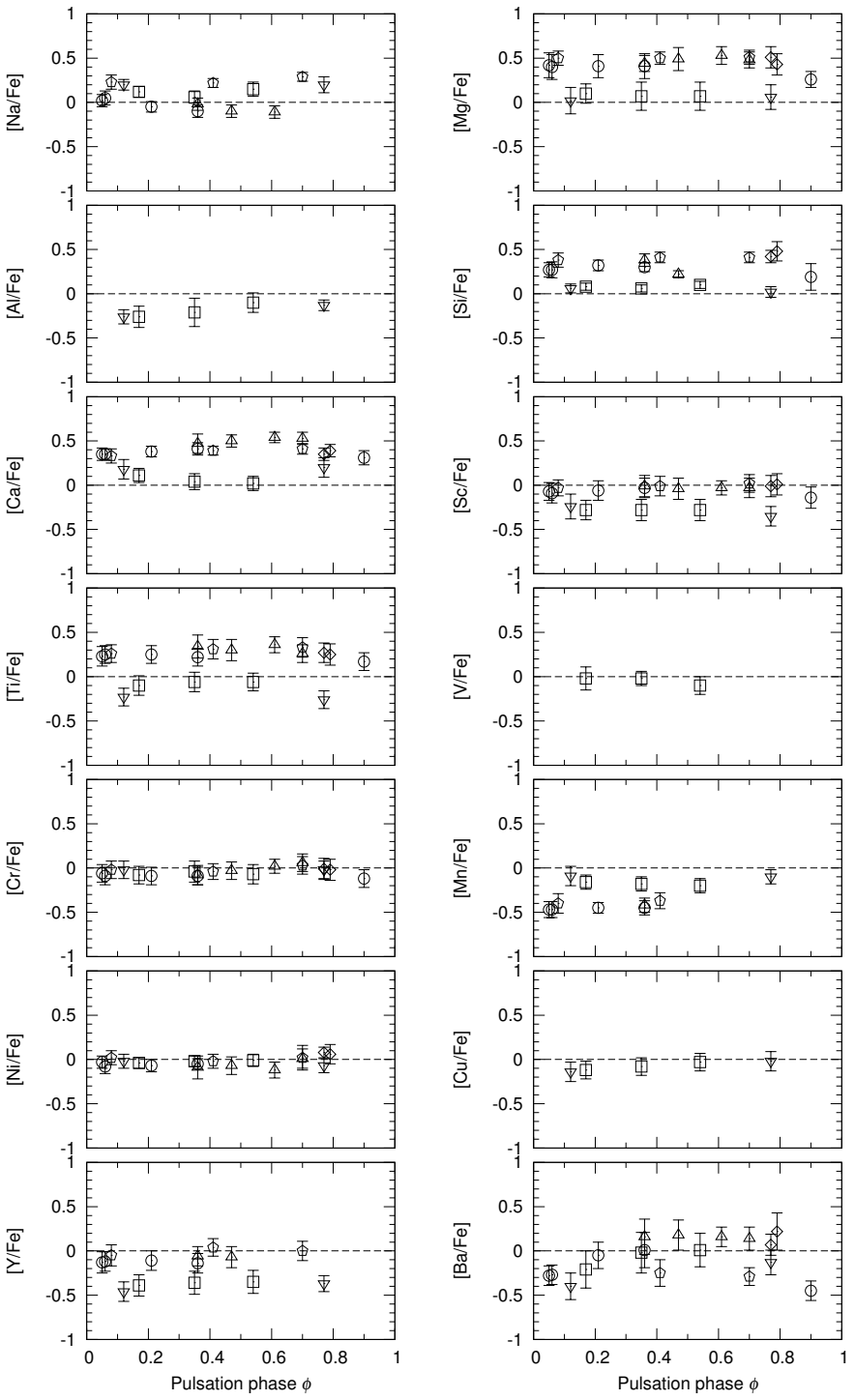

Fig. 4 Elemental abundances as a function of phase for six RR Lyrae stars with multiple observations (AO Peg: open diamonds; DH Peg: open pentagons; DX Del: open squares; RR Lyr: open circles; V445 Oph: open inverted triangles; VY Ser: open triangles).

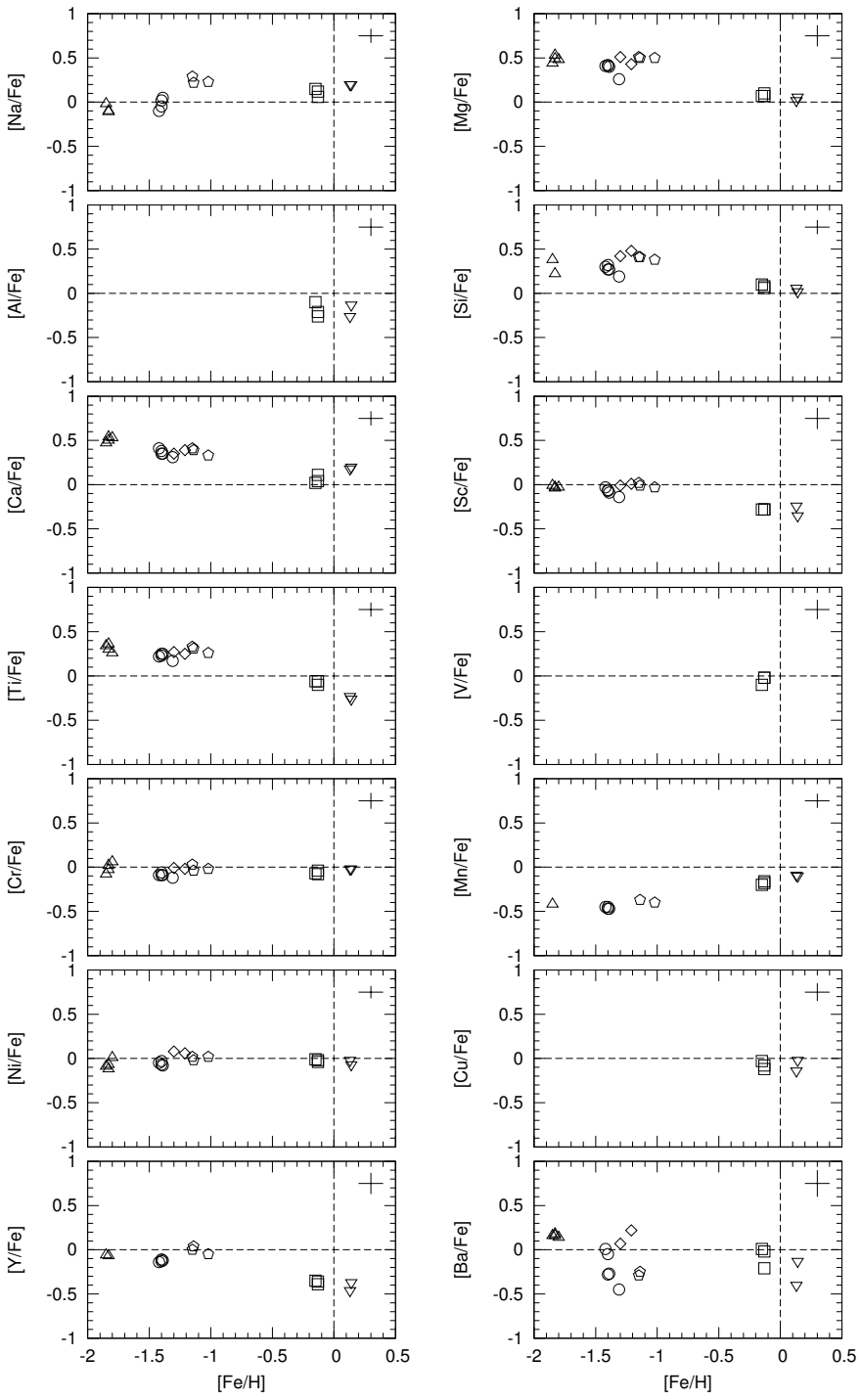

Fig. 5 Elemental abundances as a function of metallicity for six RR Lyrae stars with multiple observations. The symbols are the as same as in Fig. 4.

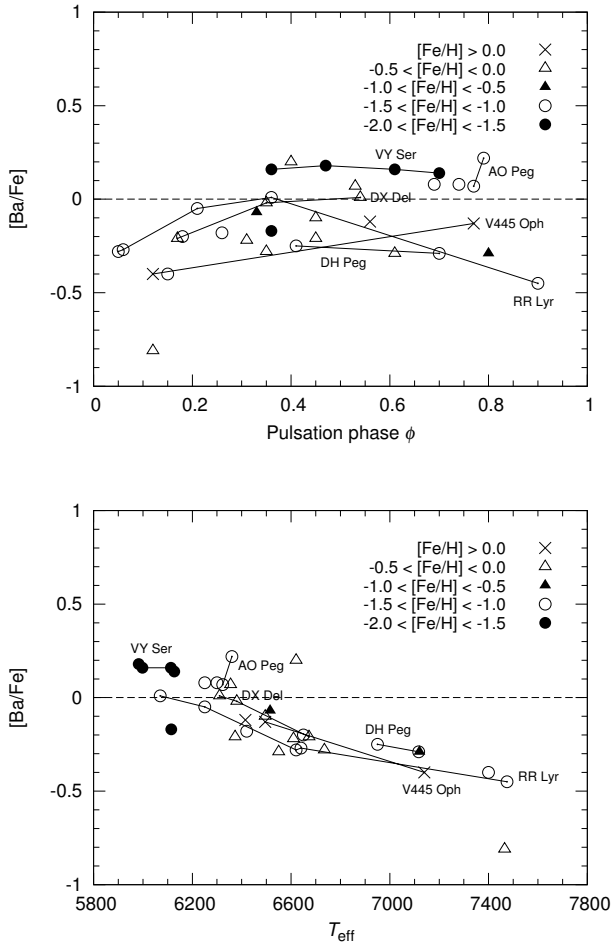

Fig. 6 The upper and lower panels show [Ba/Fe] ratios as functions of phase and $T_{\rm eff}$, respectively. Different symbols indicate different metallicity ranges. Different phases for the same star are connected by a straight line.

is caused by the possible effect of NLTE being around 0.1; this is too small to explain the deviation of 0.7 in our work. Further studies on Ba abundances for RR Lyrae stars are needed.

4.3 [X/Fe] versus [Fe/H] for All Stars in our Study

As discussed in Section 4.1, RR Lyrae stars can be used to trace the chemical evolution of the Galaxy. In Table 7, we present elemental abundances for 17 stars in our study which have one spectrum, as well as the mean [X/Fe] ratios of different phases for the six stars with observations in multiple phases. The abundance ratios as a function of metallicity for a large metallicity range of $-1.85 <$ [Fe/H] < 0.14 are displayed in Figure 7. We overplotted the abundance results of dwarfs by Reddy et al. (2006). In addition, abundance results of RR Lyrae stars from Clementini et al. (1995) and For et al. (2011) are also plotted for comparison. Below, we will describe the abundance patterns of RR Lyrae stars for four groups of elements.

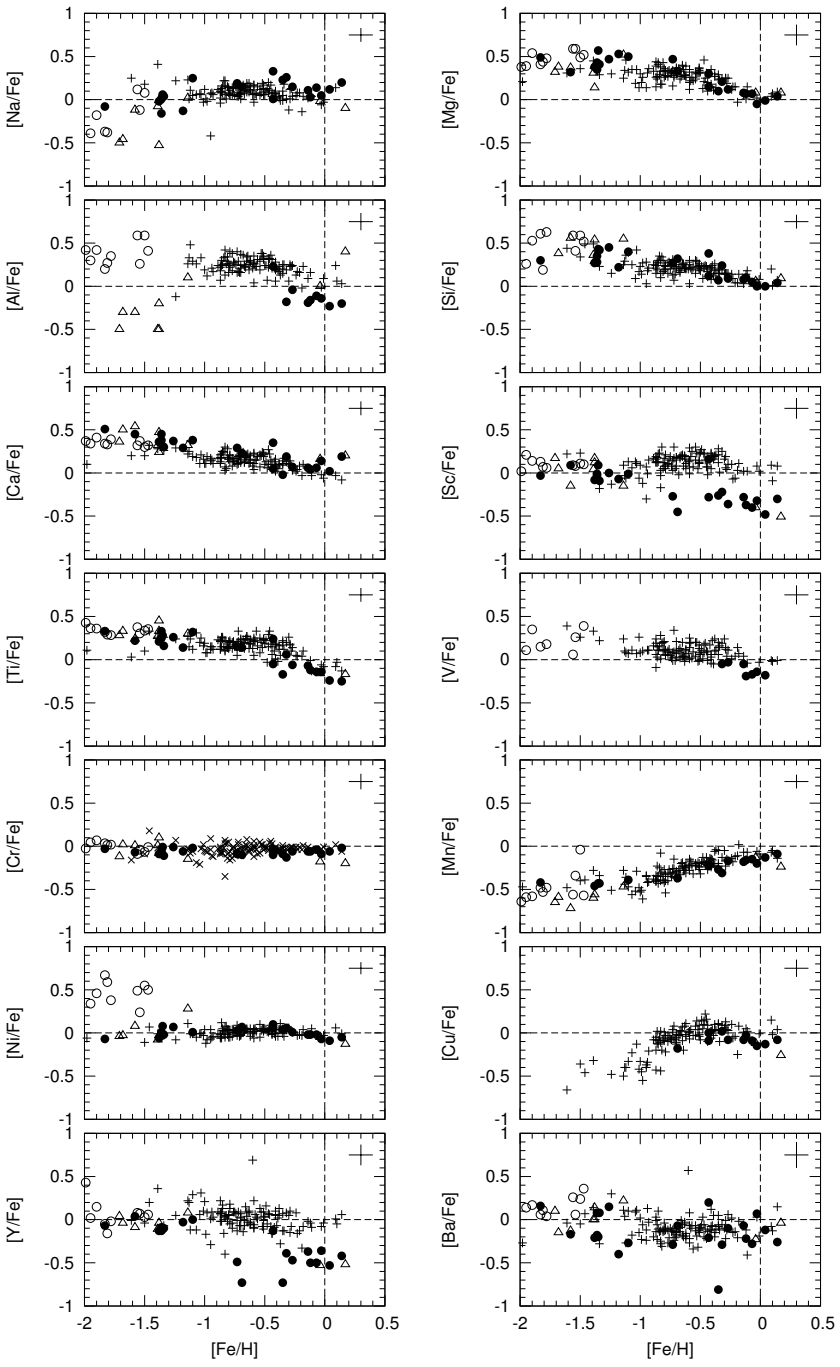

Fig. 7 Elemental abundances relative to iron abundances. The [X/Fe] ratios in this work are indicated by filled circles. Stars from Reddy et al. (2006) are represented by pluses. Metal-poor RR Lyrae stars from For et al. (2011) are marked by open circles. Open triangles refer to RR Lyrae stars from Clementini et al. (1995).

Table 7 Derived abundances for the 23 sample stars; mean abundances of different phases for six stars are adopted.

Star	[Fe/H]	[α/Fe]	[Na/Fe]	[Mg/Fe]	[Al/Fe]	[Si/Fe]	[Ca/Fe]	[Sc/Fe]	[Ti/Fe]	[V/Fe]	[Cr/Fe]	[Mn/Fe]	[Ni/Fe]	[Cu/Fe]	[Y/Fe]	[Ba/Fe]
AA Aql	−0.32	0.17	0.26	0.21	−0.18	0.24	0.19	−0.22	0.06	−0.05	−0.13	−0.31	0.06	0.02	−0.39	−0.29
AO Peg	−1.26	0.38	...	0.47	...	0.45	0.37	0.00	0.26	...	−0.01	...	0.07	...	...	0.15
BR Aqr	−0.69	0.25	0.15	0.33	...	0.32	0.23	−0.45	0.14	...	−0.10	−0.37	0.07	−0.18	−0.73	−0.07
CI And	−0.43	0.06	0.01	0.15	...	0.12	0.05	−0.28	−0.05	...	−0.10	−0.21	0.06	−0.09	...	−0.21
CN Lyr	−0.04	−0.02	0.05	−0.05	−0.14	0.00	0.14	−0.32	−0.14	−0.14	−0.09	−0.20	−0.07	−0.15	−0.36	0.07
DH Peg	−1.09	0.39	0.25	0.50	...	0.40	0.38	−0.01	0.32	...	−0.02	−0.39	0.01	...	0.00	−0.27
DM Cyg	0.03	−0.07	0.12	−0.01	−0.23	0.00	0.02	−0.48	−0.24	−0.18	−0.06	−0.13	−0.09	−0.13	−0.53	−0.12
DO Vir	−1.57	0.32	...	0.32	...	...	0.45	0.09	0.22	...	−0.07	...	...	...	0.04	−0.17
DX Del	−0.14	0.03	0.11	0.08	−0.19	0.08	0.06	−0.28	−0.07	−0.05	−0.06	−0.18	−0.02	−0.08	−0.37	−0.07
IO Lyr	−1.35	0.35	0.01	0.43	...	0.35	0.38	−0.03	0.25	...	−0.07	...	0.01	...	−0.13	−0.18
KX Lyr	−0.27	0.05	0.15	0.12	−0.04	0.09	0.07	−0.36	−0.06	−0.03	−0.06	−0.17	0.01	−0.08	−0.47	−0.10
RR Cet	−1.34	0.39	0.06	0.57	...	0.43	0.31	0.09	0.28	...	−0.01	−0.43	0.08	...	−0.11	−0.20
RR Lyr	−1.38	0.30	−0.02	0.38	...	0.27	0.36	−0.08	0.21	...	−0.09	−0.46	−0.06	...	−0.13	−0.21
RS Boo	−0.12	0.02	0.03	0.07	−0.16	0.10	0.04	−0.37	−0.12	−0.19	−0.06	−0.16	−0.02	−0.03	−0.50	−0.22
SW And	−0.07	0.00	0.14	0.07	−0.11	0.05	0.06	−0.40	−0.14	−0.17	−0.04	−0.15	−0.02	−0.09	−0.50	−0.28
TV Lib	−0.43	0.28	0.28	0.30	0.23	0.27	0.35	0.12	0.24	...	−0.03	−0.23	0.10	0.00	−0.13	0.20
TW Her	−0.35	−0.01	0.23	0.10	...	0.07	−0.02	−0.26	−0.17	...	−0.09	−0.27	0.04	...	−0.73	−0.81
UU Cet	−1.36	0.35	−0.16	0.35	...	0.28	0.45	−0.01	0.33	...	−0.06	...	...	...	−0.09	0.08
V413 Oph	−0.75	0.29	0.19	0.47	...	0.27	0.29	−0.27	0.15	...	−0.09	...	0.03	...	−0.49	−0.29
V440 Sgr	−1.18	0.29	−0.13	0.53	...	0.22	0.29	−0.07	0.14	...	−0.06	...	...	...	−0.03	−0.40
V445 Oph	0.14	0.00	0.20	0.04	−0.20	0.04	0.19	−0.30	−0.25	...	−0.02	−0.09	−0.05	−0.08	−0.42	−0.26
VX Her	−1.33	0.32	0.04	0.41	...	0.42	0.30	−0.09	0.16	...	−0.11	−0.43	−0.02	...	−0.10	0.08
VY Ser	−1.83	0.40	−0.08	0.49	...	0.30	0.51	−0.03	0.33	...	−0.03	−0.42	−0.07	...	−0.07	0.16

4.3.1 The α-elements

In Figure 7, the four α-elements (Mg, Si, Ca, and Ti) exhibit a decreasing trend with increasing metallicity. Specifically, there is an overabundant [α/Fe] of 0.34 in the moderately metal-poor range of $-1.85 <$ [Fe/H] < -0.70. For [Fe/H] > -0.70, the trend decreases steeply with increasing metallicity until reaching the solar value at [Fe/H] ~ 0.0. The abundance behaviors of α-elements generally follow the same pattern as those in dwarf stars (Bensby et al. 2003; Fulbright 2000; Reddy et al. 2006), but we note that [Ti/Fe] in this work is $0.1 - 0.2$ dex lower than abundances of three other α-elements, which is also reported by Zhang et al. (2009) for both dwarf and giant stars. A possible explanation is that the heavy α-element Ti is produced during complete and incomplete silicon burning while Si and Ca undergo incomplete explosive silicon and oxygen burning (Cayrel et al. 2004). In addition, there is slightly higher [Mg/Fe] than is seen in dwarf stars for the relatively metal-poor RR Lyrae stars at the mild metallicity range of $-1.85 <$ [Fe/H] < -0.7, indicating their possible origin from the thick disk or the halo. Later information on kinematics will help to clarify this issue.

4.3.2 The light odd-Z elements

In Figure 7, [Na/Fe] ratios show a rising trend with increasing metallicity at the metal-poor end and then become relatively flat towards higher metallicity. The [Na/Fe] behaviors of RR Lyraes are consistent with the results from giants (Alves-Brito et al. 2010) and dwarfs (Bensby et al. 2003; Fulbright 2000; Reddy et al. 2006). In this work, we adopt four Na I lines, which are the $\lambda\lambda$5682.6, 5688.2 and $\lambda\lambda$6154.2, 6160.7 doublets. The Na I resonance D-lines, $\lambda\lambda$5889.9, 5895.9, are not used to avoid severe saturation in metal-rich stars.

Al might have been expected to behave like Na. In this work, Al I lines $\lambda\lambda$6696.0, 6698.6 and $\lambda\lambda$7835.3, 7836.1 are adopted. Since the lines are too weak to be detected in our metal-poor stars, Al abundances are derived for eight metal-rich RR Lyraes and result in a mean [Al/Fe] of -0.11. TV Lib shows a large deviation by having an overabundant [Al/Fe] of 0.23 while the other eight metal-rich variables have underabundant [Al/Fe]. Note that TV Lib also shows obvious high abundances for Sc, Y and Ba elements, and will be discussed as a special case in Section 4.5.

Sc abundances in this study show a decreasing trend with increasing metallicity. As exhibited in Figure 7, [Sc/Fe] shows a nearly flat behavior with the solar value in a mildly metal-poor range of $-1.85 <$ [Fe/H] < -0.70, and then starts to decrease at [Fe/H] ~ -0.70 with an underabundant [Sc/Fe] of -0.32 for 13 stars in the metal-rich end. Obviously, Sc abundances follow the same pattern as α-elements, which was suggested by Nissen et al. (2000). However, our [Sc/Fe] ratios have significantly lower ratios at the metal-rich end, and interestingly, there is a similar case — Yttrium, which is shown in Section 4.3.4. The interpretation for the peculiar Sc and Y abundances will be presented later in the description of Y abundance.

4.3.3 The iron-peak elements

The iron-peak elements have a similar nucleosynthesis process that is mainly produced by an SN Ia, and they are believed to show the same abundance patterns as iron. [X/Fe] ratios of iron-peak elements, V, Cr, Mn, Ni and Cu, as a function of metallicity are exhibited in Figure 7.

The Cr and Ni show a similar trend that closely follows Fe over the whole metallicity range of $-1.85 <$ [Fe/H] < 0.14, which is in good agreement with of those of giants and dwarfs (Chen et al. 2000; Fulbright 2000; Reddy et al. 2006; Takeda et al. 2008).

[Mn/Fe] in our analysis presents an increasing trend with increasing metallicity. The flat trend with underabundant [Mn/Fe] ~ -0.43 at the metal-poor end of [Fe/H] < -1.0 is consistent with the results of Mn in dwarfs (Gratton 1989; Nissen et al. 2000; Reddy et al. 2006).

The abundances of V and Cu are only derived for metal-rich RR Lyrae variables. Abundances of the two elements shown in Figure 7 are both approximately constant around the solar values for [Fe/H] > -0.80, with a mean [V/Fe] of -0.11 and a mean [Cu/Fe] of -0.08. Both of the trends generally confirm the trends of V or Cu for dwarfs (Reddy et al. 2006).

4.3.4 The neutron capture elements

At solar and moderately low metallicity, the slow neutron capture process (s-process) dominates the abundances of Y and Ba (Arlandini et al. 1999). The s-process, which has a typical neutron capture timescale that is longer than the timescale of β-decay, probably occurs in the convection zone of low mass asympototic giant branch (AGB) stars on a similar timescale as the iron-peak elements produced in SNe Ia.

As mentioned above, [Y/Fe] shows the α-element-like trend following [Sc/Fe]. As compared with the flat pattern around the solar value of Y for dwarfs with [Fe/H] < -1.0 (Reddy et al. 2006; Zhao & Magain 1991), Y gives significantly lower abundances with a mean [Y/Fe] of -0.47 in the metallicity range of [Fe/H] > -0.7.

The anomalous abundances of Sc and Y in metal-rich RR Lyrae stars are unexplained in the context of Galactic chemical evolution. Clementini et al. (1995) is the only study which has reported the underabundant [Sc/Fe] and [Y/Fe]. For two common stars, SW And and V445 Oph, Clementini et al. (1995) derived the mean [Sc/Fe] = -0.51 and [Y/Fe] = -0.47 while the mean [Sc/Fe] and [Y/Fe] of our work are -0.35 and -0.46 respectively. Clementini et al. (1995) suspected that the anomalous abundances of Sc and Y are attributed to overionization caused by the Lyman line emission that is induced by a shock wave during the pulsation cycle. However, it is not clear why the effect of low Sc and Y abundances is not found in metal-poor stars. Alternatively, we note that Sc and Y abundances are derived with ionized lines, which are sensitive to surface gravity as shown in Tables 4 and 5. In view of this, we consider that the deviations could come from different surface gravities between evolved RR Lyrae stars and unevolved dwarf stars. We thus suggest that they may not represent the chemical evolution of the Galaxy.

As already discussed in Section 4.2, [Ba/Fe] for stars in our study has a large star-to-star scatter of 0.22 and exhibits a slightly increasing trend with increasing [Fe/H] for the whole range of metallicity. Again, the abundance trend follows the same pattern as for dwarf stars (Fulbright 2000; Reddy et al. 2006). In addition, TW Her, the outlier with pronounced Ba underabundance of -0.81, will be discussed as a special case in Section 4.5.

4.3.5 Remarks on abundance results

In comparison with dwarf stars from the literature, we found that most elements follow similar trends, except for Sc and Y, which have significantly lower abundance ratios at metal-rich ends. The peculiar abundances of the two elements do not follow the general picture of Galactic chemical evolution.

Comparing with results on RR Lyrae stars, our elemental abundances agree with those from Clementini et al. (1995) for eight common stars. In particular, for Sc and Y, Clementini et al. (1995) also found anomalous behaviors in metal-rich RR Lyraes but did not give an explicit interpretation for the mechanism. Further studies on both observations and theory are needed.

In addition, at the metal-poor end, we included 11 field RR-ab type stars from For et al. (2011) and there are consistent trends for most elements. For example, decreasing [Na/Fe] with decreasing metallicity is seen in both works, but the enhanced [Ni/Fe] ratios in For et al. (2011) are not found in our data and are unexplained by the nuclosynthesis that predicts the same yield for Fe and Ni.

4.4 Kinematics

The kinematic parameters ($U_{\rm LSR}$, $V_{\rm LSR}$, $W_{\rm LSR}$), relative to the local standard of rest (LSR), were derived based on the method given by Johnson & Soderblom (1987), adopting the correction for solar motion of $(-8.50, +13.38, +6.49)$ km s^{-1} (Coşkunoğlu et al. 2011). The radial velocity was measured from our spectra, and corrected to the heliocentric velocities. The position, distance and proper motion were taken from Beers et al. (2000). Mean values of kinematic parameters from different phases for the RR Lyraes, with observations that included multiple phases, were adopted to represent their kinematics.

We then followed the method adopted by Reddy et al. (2006) of assigning the probability of membership for each star to either the halo, the thick disk or the thin disk. In Reddy et al. (2006), stars in the halo, thick-disk and thin-disk are assumed to follow a Gaussian distribution function in Galactic velocity space (U, V, W). With given asymmetric velocity drifts and dispersions, the probability that a star belongs to the halo ($P_{\rm halo}$), the thick disk ($P_{\rm thick}$) or the thin disk ($P_{\rm thin}$) could be computed. A probability in excess of 70 percent was considered to assign a star to either the halo, the thick disk, or the thin disk. Of the 23 field RR Lyraes, seven variables belong to the halo population, three variables to the thick disk and 10 variables were classified as thin disk stars. For the remaining three stars, BR Aqr and TV Lib belong to either the thin or thick disk with approximately equal probability or probability lower than 70 percent, while V440 Sgr belongs to either the thick disk or halo with equal probability. All the stars in our study are plotted on the Toomre diagram in Figure 8, and are listed by different classifications in the last column of Table 8, in addition to their kinematic parameters mentioned above.

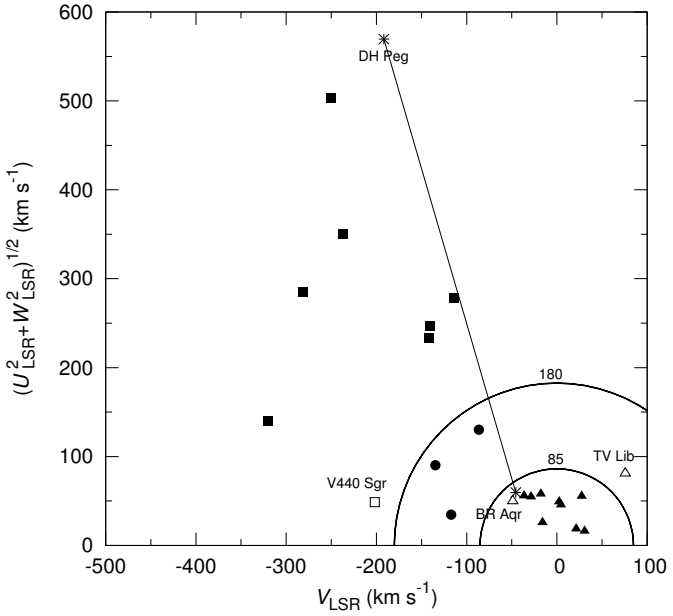

Fig. 8 Toomre diagram of the stars in our study. The halo stars are represented by filled squares. The stars in the thick disk and thin disk are shown by filled circles and filled triangles respectively. The thick/thin disk stars, BR Aqr and TV Lib, are represented by open triangles; while the halo/thick disk star, V440 Sgr, is displayed by an open square. For the exception DH Peg, results calculated from two sets of different kinematics are shown by asterisks and connected by a straight line.

Table 8 Spatial velocities, population probability and kinematical classifications of stars in our study. The kinematic parameters listed in this table are calculated from data of Beers et al. (2000).

Star	$U_{\rm LSR}$ (km s^{-1})	$V_{\rm LSR}$ (km s^{-1})	$W_{\rm LSR}$ (km s^{-1})	$P_{\rm halo}$ (%)	$P_{\rm thick}$ (%)	$P_{\rm thin}$ (%)	Classification
AA Aql	-113.84	-86.41	62.96	3 ± 2	96 ± 0	1 ± 0	Thick Disk
AO Peg	-139.62	-320.20	13.69	99 ± 0	0 ± 0	0 ± 0	Halo
BR Aqr	3.99	-48.99	-49.68	2 ± 0	51 ± 7	47 ± 62	Thin Disk/Thick Disk
CI And	12.04	21.24	-14.25	0 ± 0	1 ± 0	99 ± 0	Thin Disk
CN Lyr	-55.44	27.46	0.16	0 ± 0	1 ± 0	99 ± 0	Thin Disk
DH Peg	55.16	-45.47	22.54	0 ± 0	8 ± 2	92 ± 5	Thin Disk†
DM Cyg	37.02	4.57	-26.99	0 ± 0	3 ± 0	96 ± 2	Thin Disk
DO Vir	398.62	-250.14	306.90	99 ± 0	0 ± 0	0 ± 0	Halo
DX Del	57.47	-17.83	7.55	0 ± 0	2 ± 1	98 ± 1	Thin Disk
IO Lyr	257.59	-113.88	106.56	97 ± 3	3 ± 7	0 ± 0	Halo
KX Lyr	-55.06	-36.45	8.96	0 ± 0	3 ± 3	97 ± 12	Thin Disk
RR Cet	-85.62	-134.65	28.64	7 ± 1	93 ± 3	1 ± 0	Thick Disk
RR Lyr	246.25	-140.10	3.56	85 ± 8	15 ± 14	0 ± 0	Halo
RS Boo	-13.97	30.69	-8.14	0 ± 0	1 ± 0	99 ± 0	Thin Disk
SW And	-52.56	-28.78	-15.03	0 ± 0	3 ± 0	97 ± 2	Thin Disk
TV Lib	80.44	75.57	-9.85	0 ± 0	15 ± 25	85 ± 50	Thin Disk/Thick disk
TW Her	-11.07	-16.07	-23.27	0 ± 0	2 ± 0	98 ± 2	Thin Disk
UU Cet	228.77	-142.27	45.25	84 ± 12	16 ± 25	0 ± 0	Halo
V413 Oph	-34.16	-117.26	5.98	2 ± 1	89 ± 10	9 ± 41	Thick Disk
V440 Sgr	43.12	-201.78	-22.62	56 ± 1	44 ± 42	0 ± 0	Thick Disk/Halo
V445 Oph	28.70	2.44	39.81	0 ± 0	7 ± 4	93 ± 14	Thin Disk
VX Her	349.90	-237.10	-11.42	99 ± 0	0 ± 0	0 ± 0	Halo
VY Ser	257.83	-281.68	120.75	99 ± 0	0 ± 0	0 ± 0	Halo

† DH Peg is re-classified as a halo star with Hipparcos data (van Leeuwen 2007).

In Figure 8, we see that stars in the halo, as well as those in the thick and thin disk, comform well to the kinematical definition that stars with total space velocity of 85 km s^{-1} $< V_{\rm tot} <$ 180 km s^{-1} generally belong to the thick disk, stars with a velocity higher than $V_{\rm tot} > 180$ km s^{-1} and those with a velocity lower than $V_{\rm tot} < 85$ km s^{-1} have a high probability of belonging to the halo and the thin disk, respectively (Bensby et al. 2010; Fuhrmann 2004). Combining with the abundance indicator, we clearly see that halo and thick disk RR Lyrae stars classified by kinematics belong to the metal-poor group with overabundant [α/Fe] of 0.35 and 0.28, respectively. [Mg/Fe] gives similar values around 0.40 in both the halo and the thick disk RR Lyrae stars. All the thin disk stars of our sample are metal-rich RR Lyraes with [Fe/H] > -0.50. They have [α/Fe] = 0.02 and [Mg/Fe] = 0.08. There is one exception in the classification based on kinematics and metallicity. DH Peg is a metal-poor RR Lyrae star with [Fe/H] = -1.09 and an overabundant [α/Fe] = 0.39 ([Mg/Fe] = 0.50), but it is classified as a thin disk star based on Beers et al. (2000)'s kinematic data. We thus adopted the parallaxes and proper motions from newly released Hipparcos data (van Leeuwen 2007) to recalculate ($U_{\rm LSR}$, $V_{\rm LSR}$, $W_{\rm LSR}$) and applied the kinematical classification to 15 stars. The remaining eight variables are not included in the Hipparcos catalogs. The recalculated results are consistent with the calculations from data of Beers et al. (2000), except for DH Peg, which was assigned to be a member of the halo population by adopting Hipparcos data. Thus DH Peg is a halo star, instead of a thin disk star, as also indicated by its abundance pattern.

To sum up, stars in our study with halo and thick disk kinematics show enhanced [α/Fe] $\sim$ 0.30, while stars with solar [α/Fe], especially [Mg/Fe], are mainly concentrated in the metal-rich part of [Fe/H] > -0.50 and they generally have a high probability of belonging to the thin disk.

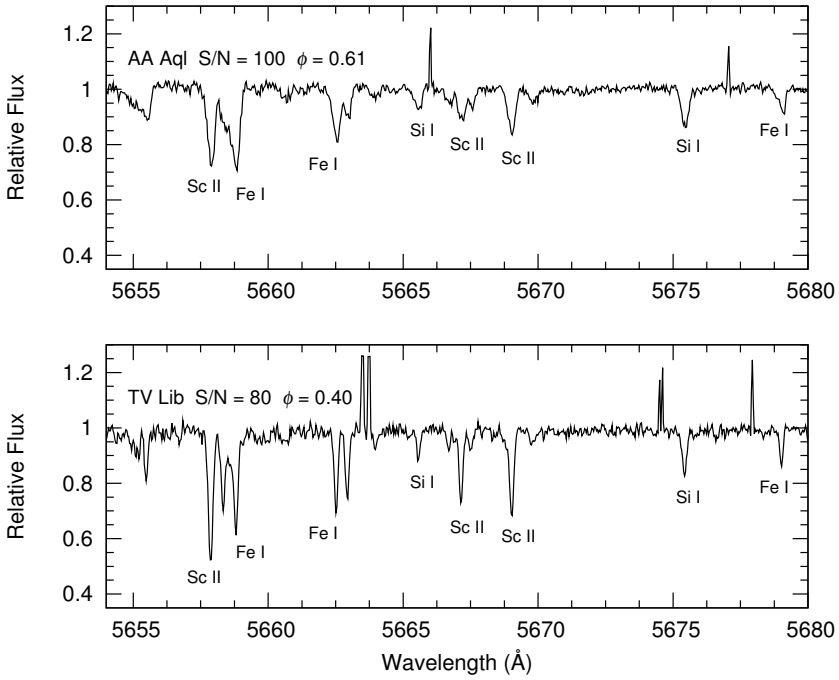

Fig. 9 Sample spectra of AA Aql and TV Lib in the section of Sc II lines at 5657.90 Å, 5667.15 Å and 5669.042 Å.

4.5 Two Special Cases — TV Lib and TW Her

Among the stars in our study, two variables, TV Lib and TW Her, have very different abundance patterns at similar metallicity around [Fe/H] = -0.4. TV Lib has overabundant [α/Fe] ratios while TW Her has solar [α/Fe] ratios. The kinematic information indicates a thick disk origin for TV Lib and a thin disk origin for TW Her. Furthermore, there are quite different abundance ratios in Sc, Y and Ba elements with the underabundant [X/Fe] ratios in TW Her. Both stars are different from other RR Lyrae stars with similar kinematics. In particular, TV Lib shows solar [Sc/Fe] following dwarf stars while other metal-rich RR Lyrae stars have underabundant [Sc/Fe] for their metallicity. We have shown the spectra, including three Sc II lines in Figure 9, and they indeed have stronger lines as compared with AA Aql, which has similar atmospheric parameters as TV Lib. Although TV Lib only has a slightly lower microturbulent velocity, [Sc/Fe] is not sensitive to the microturbulence. We suspect that the enhanced [Sc/Fe] in this star is real. In addition, we note that TV Lib has an extremely short period of P = 0.27 day compared with other normal RRab variables. Also, Kovács (2005) identified the short period RRab star TV Lib as an outlier in a study of the light curves of RR Lyrae variables and thought this sample might be unique. Further study on the two stars is desirable.

5 CONCLUSIONS

We derived stellar atmospheric parameters ($T_{\rm eff}$, $\log g$, [Fe/H], $v_{\rm t}$) and abundance ratios [X/Fe] for 15 elements in a sample of 23 RR Lyrae stars. Among the sample stars, six have spectra at different phases, and we found consistent abundance ratios without any trend in different phases, which was

previously investigated in the metal-poor population for a limited number of stars. We confirmed that RR Lyrae stars are good stellar tracers of Galactic chemical evolution by extending the study to metal-rich populations until [Fe/H] > 0.0 and to more elements. Their abundances generally follow the same trends as dwarf stars except for Sc and Ba. The kinematics indicate their origins are from a mixture of three populations (the halo, the thick disk and the thin disk), while the metal-rich RR Lyrae stars with [Fe/H] > -0.5 tend to originate from the thin disk. In addition, we found a complicated behavior in [Ba/Fe], which has a large scatter at a given metallicity and an interesting dependence on temperature for the same metallicity range. Finally, we found two special stars, TV Lib and TW Her, which have different abundance patterns, indicating that some special processes have happened in some RR Lyrae stars.

Acknowledgements We thank Prof. Xiaobin Zhang for valuable suggestions on determination of the pulsation ephemeris for RR Lyrae stars. We thank Dr. Kefeng Tan, Dr. Liang Wang and Dr. Xiangxiang Xue for constructive suggestions. This study is supported by the National Natural Science Foundation of China (Grant Nos. 11233004, 11222326 and 11073026).

References

Alves-Brito, A., Meléndez, J., Asplund, M., Ramírez, I., & Yong, D. 2010, A&A, 513, A35
Andrievsky, S. M., Spite, M., Korotin, S. A., et al. 2009, A&A, 494, 1083
Arlandini, C., Käppeler, F., Wisshak, K., et al. 1999, ApJ, 525, 886
Beers, T. C., Chiba, M., Yoshii, Y., et al. 2000, AJ, 119, 2866
Bensby, T., Alves-Brito, A., Oey, M. S., Yong, D., & Meléndez, J. 2010, A&A, 516, L13
Bensby, T., Feltzing, S., & Lundström, I. 2003, A&A, 410, 527
Castelli, F., & Kurucz, R. L. 2003, in Modelling of Stellar Atmospheres, IAU Symposium, 210, eds. N. Piskunov, W. W. Weiss, & D. F. Gray, 20P
Cayrel, R., Depagne, E., Spite, M., et al. 2004, A&A, 416, 1117
Chen, Y. Q., Nissen, P. E., Zhao, G., Zhang, H. W., & Benoni, T. 2000, A&AS, 141, 491
Clementini, G., Carretta, E., Gratton, R., et al. 1995, AJ, 110, 2319
Coşkunoğlu, B., Ak, S., Bilir, S., et al. 2011, MNRAS, 412, 1237
Cunha, K., Smith, V. V., Bergemann, M., Suntzeff, N. B., & Lambert, D. L. 2010, ApJ, 717, 333
Fernley, J., & Barnes, T. G. 1996, A&A, 312, 957
For, B.-Q., Sneden, C., & Preston, G. W. 2011, ApJS, 197, 29
Fuhrmann, K. 2004, Astronomische Nachrichten, 325, 3
Fulbright, J. P. 2000, AJ, 120, 1841
Gratton, R. G. 1989, A&A, 208, 171
Johnson, D. R. H., & Soderblom, D. R. 1987, AJ, 93, 864
Kolenberg, K., Fossati, L., Shulyak, D., et al. 2010, A&A, 519, A64
Kovács, G. 2005, A&A, 438, 227
Kurucz, R. 1993, ATLAS9 Stellar Atmosphere Programs and 2 km/s grid. Kurucz CD-ROM No. 13. Cambridge, Mass.: Smithsonian Astrophysical Observatory
Kurucz, R. L., Furenlid, I., Brault, J., & Testerman, L. 1984, Solar Flux Atlas from 296 to 1300 nm
Lambert, D. L., Heath, J. E., Lemke, M., & Drake, J. 1996, ApJS, 103, 183
Layden, A. C. 1994, AJ, 108, 1016
Layden, A. C. 1995a, AJ, 110, 2312
Layden, A. C. 1995b, AJ, 110, 2288
Layden, A. C., Hanson, R. B., Hawley, S. L., Klemola, A. R., & Hanley, C. J. 1996, AJ, 112, 2110
Mashonkina, L., Gehren, T., & Bikmaev, I. 1999, A&A, 343, 519
Mishenina, T. V., Kučinskas, A., Andrievsky, S. M., et al. 2009, Baltic Astronomy, 18, 193

Nissen, P. E., Chen, Y. Q., Schuster, W. J., & Zhao, G. 2000, A&A, 353, 722
Noguchi, K., Aoki, W., Kawanomoto, S., et al. 2002, PASJ, 54, 855
Preston, G. W. 1959, ApJ, 130, 507
Prochaska, J. X., Naumov, S. O., Carney, B. W., McWilliam, A., & Wolfe, A. M. 2000, AJ, 120, 2513
Reddy, B. E., Lambert, D. L., & Allende Prieto, C. 2006, MNRAS, 367, 1329
Skarka, M. 2013, A&A, 549, A101
Takeda, Y., Honda, S., Aoki, W., et al. 2006, PASJ, 58, 389
Takeda, Y., Sato, B., & Murata, D. 2008, PASJ, 60, 781
van Leeuwen, F. 2007, A&A, 474, 653
Zhang, L., Ishigaki, M., Aoki, W., Zhao, G., & Chiba, M. 2009, ApJ, 706, 1095
Zhao, G., & Magain, P. 1991, A&A, 244, 425